Micellar Solutions of a Symmetrical Amphiphilic ABA Triblock Copolymer with a Temperature-Responsive Shell

A. Jain,[1] *A. Kulkarni,*[1] *A. M. Bivigou Koumba,*[2] *W. Wang,*[1] *P. Busch,*[3] *A. Laschewsky,*[2] *P. Müller-Buschbaum,*[1] *C. M. Papadakis**[1]

Summary: We have studied the thermal behavior of an ABA triblock copolymer having short, deuterated polystyrene end-blocks and a longer poly(N-isopropyl acrylamide) middle block, the latter exhibiting a lower critical solution temperature. The collapse of the micelles was investigated using dynamic light scattering. Small-angle neutron scattering with contrast matching allowed us to quantify the core-shell structure of the micelles as well as their correlations as a function of temperature.

Keywords: amphiphiles; colloids; dynamic light scattering; micelles; small-angle neutron scattering; stimuli-sensitive polymers

Introduction

Stimuli-responsive polymeric hydrogels have received increasing attention as they respond in a controlled and reversible way with a volume change to a weak external stimulus, such as temperature, light, electric or magnetic fields, or ionic strength.[1] Especially temperature-sensitive polymers are of great interest for medical and drug delivery applications, bio-separation and diagnostics,[2–4] as well as for porous membranes for molecular filtration where the permeability can be controlled by a change of temperature across the lower critical solution temperature (LCST).[5–7] Polymers with an LCST behavior, i.e. a temperature-dependent solubility in water, are attractive candidates: they are swollen below the LCST and collapsed, i.e. water-insoluble, above. A widely used LCST polymer is poly(N-isopropyl acrylamide) (PNIPAM). Its LCST at 32 °C is attributed to alterations in the hydrogen-bonding interactions of the amide group.[8–10] So far, macroscopic gels,[11–13] microgels,[14–17] and core-shell lattices with a cross-linked hydrophobic core and a cross-linked responsive shell[18–21] have been studied.

The hydrophobic modification of both ends of PNIPAM by alkyl end-groups[22,23] or the use of block copolymers with one or two hydrophobic blocks and a PNIPAM block [7,24–30] are alternative routes to the formation of temperature-responsive micelles or micellar gels, where the ability to self-organize in aqueous solution is exploited. ABA triblock copolymers consisting of a PNIPAM middle block and polystyrene (PS) end-blocks were reported to form flower-like micelles in water which collapse at the LCST of PNIPAM.[28] In very dilute solutions, it was found that the magnitude of the size decrease depends on the volume fraction of PNIPAM.[28] Polymers with high PNIPAM content were reported to take up large amounts of water upon immersion in water below the LCST.[7]

In the present work, we have investigated micellar solutions of an ABA triblock copolymer consisting of a long PNIPAM

[1] Physikdepartment E13, Technische Universität München, James-Franck-Str. 1, 85747 Garching, Germany
Fax: (+49) 89 289 12 447;
E-mail: Christine.Papadakis@ph.tum.de
[2] Institut für Chemie, Universität Potsdam, Karl-Liebknecht-Str. 24-25, 14476 Golm/Potsdam, Germany
[3] Jülich Centre for Neutron Science at FRM II, Forschungszentrum Jülich. Lichtenbergstr. 1, 85747 Garching, Germany

middle block and two short PS end-blocks. Using turbidimetry as well as temperature-resolved dynamic light scattering (DLS) and small-angle neutron scattering (SANS), we show that, in aqueous solution, these copolymers form spherical micelles of core-shell type, which collapse at the LCST of PNIPAM and aggregate to large clusters consisting of collapsed micelles.

Experimental Part

The polymer was prepared by successive RAFT polymerization of styrene-d_8, using dibenzyltrithiocarbonate as bifunctional chain transfer agent, and subsequent chain extension with N-isopropylacrylamide (NIPAM). Details of the synthesis and molecular characterization will be reported elsewhere.

Turbidity measurements were performed on a temperature-controlled turbidimeter (model TP1, E. Tepper, Germany) with heating and cooling rates of 1.0 K min^{-1}, respectively. The transmittance of the polymer solution was set to 90% at the beginning of each measurement. Temperatures are precise within 0.5 K.

The polymer aggregation in aqueous solution was followed by DLS. Temperature-resolved experiments on a filtered solution of 0.2 mg mL^{-1} were performed in polarized geometry using an ALV-5000/E correlator together with a goniometer with an index matching vat filled with toluene. The light source was a Nd:YAG laser operated at $\lambda = 532$ nm. The scattered light was detected at a scattering angle $\theta = 90^\circ$ using the setup described previously.[30] At each temperature, 3 measurements of 3 min duration were performed. After each temperature change, the waiting time was 20 min. The average hydrodynamic radii of the micelles or the clusters, R_h, were determined by cumulant analysis of the correlation functions. Moreover, the correlation curves were analyzed using the routine REPES,[31] as detailed in Ref. 30, which gives distribution functions of hydrodynamic radii. Additional experiments were performed on filtered solutions of 1 mg mL^{-1} (WICOM OPTI-Flow 0.45 μm disposable filter) using a high-performance particle sizer (HPPS-ET, Malvern Instruments, UK) equipped with a He-Ne laser ($\lambda = 633$ nm) and a thermoelectric Peltier temperature controller. The measurements were made at $\theta = 173^\circ$ (''backscattering detection''). For each measurement, the optimum measurement position, i.e. the optimal distance of the focal point from the cuvette wall, and the optimal attenuation were determined automatically by the HPPS software (Dispersion Technology software 4.0). The autocorrelation functions were analyzed with the CONTIN method. The average Rh–values were calculated according to the Stokes-Einstein equation, $R_h = k_B\ T/(6\pi\eta D_{app})$, with D_{app} being the apparent diffusion coefficient and η the viscosity of the solution.

SANS experiments were carried out at KWS-2 at the FRM-II, Garching, Germany. A wavelength, $\lambda = 0.7$ nm ($\Delta\lambda/\lambda = 20\%$) and sample-to-detector distances (SDD) of 2 m and 8 m were chosen. The detector was a ^{6}Li scintillator. The samples having concentrations of 50 mg mL^{-1} and 170 mg mL^{-1} were mounted in standard Hellma quartz cuvettes (light path of 1 mm or 2 mm). For the 50 mg mL^{-1} (170 mg mL^{-1}) solution, the measuring times per image were 10 min (5 min) for SDD = 2 m and 20 min (10 min) for SDD = 8 m. The background of the cuvette was subtracted from the sample scattering taking the transmissions into account. The intensities were corrected for dark current with boron carbide. The scattering of poly(methyl methacrylate) was used for measuring the detector sensitivity and for bringing the intensities on an absolute scale. They were azimuthally averaged using the software QtiKWS. The scattering length densities of the polymer blocks, $\delta_{P(S\text{-}d8)} = 6.42 \times 10^{10}$ cm^{-2} and $\delta_{PNIPAM} = 0.79 \times 10^{10}$ cm^{-2}, were calculated based on the scattering length densities of the elements and the mass densities. Contrast matching of the core or the shell block was performed by using either pure D_2O or a 20:80 mixture of D_2O ($\delta_{D2O} = 6.38 \times 10^{10}$ cm^{-2}) and

H_2O ($\delta_{H2O} = -0.56 \times 10^{10}\,cm^{-2}$) as a solvent. Samples were mounted in an oven with a temperature stability of 0.1 K. After each change of temperature, a waiting time of 15 min was applied to ensure thermal equilibrium. The curves were analyzed using the software Scatter 2.0.[32] A model of spherical core-shell micelles together with a Percus-Yevick structure factor was used. The incoherent background due to the solvent and the polymer was treated as a fitting parameter. In some cases, forward scattering was modeled by an algebraic decay and was subtracted before further analysis.

Results and Discussion

The Synthesis

The synthesis of the amphiphilic ABA triblock copolymer by the RAFT method using the bifunctional trithiocarbonate CTA1 is shown in Scheme 1. In the first step, styrene-d_8 is thermally polymerized in the presence of the appropriate amount of CTA1. After isolation and purification, the formed polystyrene-d_8, P(S-d_8), is engaged as bifunctional macroRAFT agent (macroCTA1) in the subsequent polymerization of NIPAM initiated by AIBN to produce the symmetrical ABA triblock copolymer P(S-d_8)-*b*-PNIPAM-*b*-P(S-d_8).

The analysis of macroCTA1 by SEC shows a monomodal, relatively narrow molar mass distribution, with a number-average molar mass M_n of 2300 g mol^{-1} (corresponding to an average degree of polymerization of 20.5), and a polydispersity index (PDI) of 1.19.

Subsequently, the P(S-d_8) was employed as bifunctional macroRAFT agent for chain-extension with NIPAM. The SEC eluogram of the ABA triblock copolymer shows a monomodal molar mass distribution with a PDI value of 1.47 and an apparent number-average molar mass $M_n^{app} = 19700\,g\,mol^{-1}$ based on calibration with PS. The determination of the absolute molar mass of the ABA triblock copolymer is inherently difficult and inaccurate, as several problems are superposed. This comprises the amphiphilic character of the block copolymer with a strong tendency to aggregate in solution, the unfavorable combination of a very large block, namely of PNIPAM, with a very short one, namely of P(S-d_8), as well as its hygroscopicity. Based on the absorbance of the P(S-d_8) block at 262 nm, an absolute molar mass of (46300 ± 13000) g mol^{-1} is calculated for the ABA triblock copolymer, assuming that the molar mass of the P(S-d_8) block of 2300 g mol^{-1} is preserved in the block copolymer. This means a number-average degree of polymerization of 389 ± 100 of the PNIPAM block.

The Collapse Transition

The thermoresponsive behavior of the amphiphilic ABA triblock copolymer was followed via the changes in light transmission (Figure 1a). A 1 mg mL^{-1} solution shows a two-step decay: Upon heating, the transmission decays abruptly from 90%, the preset value, to ~70% at 32.6 °C. Above this temperature, the decay is less steep, and the transmission reaches a plateau at 34% at ~45 °C. Upon cooling, a slight hysteresis is observed below 37 °C with a steep rise below 32.1 °C, and the curve joins the heating curve at 27 °C. This behavior is very similar to the one observed by us in an

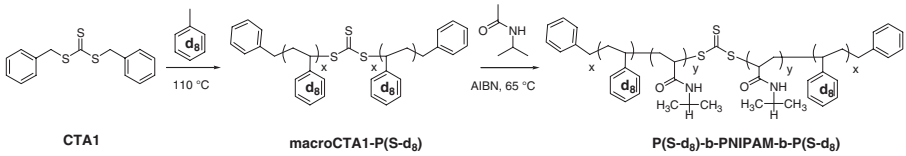

Scheme 1.
Synthesis of triblock copolymer P(S-d_8)-*b*-PNIPAM-*b*-P(S-d_8) via successive RAFT polymerizations of styrene-d_8, using CTA1, and NIPAM.

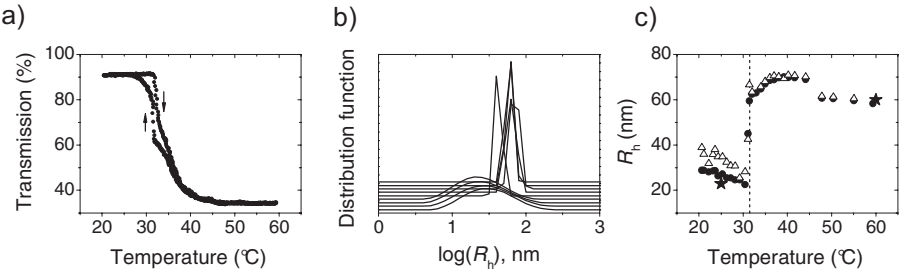

Figure 1.
(a) Temperature-dependent light transmission of a 1 mg mL^{-1} aqueous solution of P(S-d_8)-*b*-PNIPAM-P(S-d_8). Arrows mark the course of heating and cooling. (b) Distribution functions of hydrodynamic radii for 20.6 °C, 25.3 °C, 29.2 °C, 30.4 °C, 31.1 °C, 32.0 °C, 40.2 °C, 50.4 °C, 59.3 °C (from below). (c) Resulting R_h-values of the micelles: 0.2 mg mL^{-1} at $\theta = 90°$, analyzed using cumulant analysis (filled circles) and REPES (open triangles) and in a solution of 1 mg mL^{-1} at $\theta = 173°$ (stars). The dashed line marks the temperature at which the light transmission starts to decay (31.5 °C).

aqueous solution of a PS-*b*-PNIPAM diblock copolymer.[30] We conclude that the clustering of the collapsed micelles, which results in a decrease of the light transmission, proceeds in two steps. Upon cooling of PNIPAM homopolymer solutions, a two-step process was observed as well in microcalorimetry and was attributed to additional hydrogen bonds formed in the collapsed state, hindering the dissolution of PNIPAM chains.[33]

In order to characterize the collapse transition in more detail, we have carried out temperature-resolved DLS experiments. A concentration of 0.2 mg mL^{-1}, thus lower than in the turbidimetry experiment, was chosen in order to avoid multiple scattering. The resulting distributions of hydrodynamic radii are shown in Figure 1b. Below 31 °C, the distributions are broad, whereas they are shifted to higher values and become sharper above 31 °C. Because of this broadness, the average R_h-values obtained from cumulant analysis and from REPES analysis differ slightly (Figure 1c). At 21 °C, particles having a hydrodynamic radius of $R_h = 29$ nm (value from cumulant analysis) are observed, which we attribute to micelles formed by the amphiphilic ABA triblock copolymer. R_h decreases to 23 nm at 30 °C and then abruptly increases to 59 nm at 31 °C. R_h continues to increase to 69 nm in the temperature range up to 37 °C and stays at this value up to 44 °C. Above 44 °C, values around 60 nm are obtained. These values coincide with the ones obtained at 1 mg mL^{-1} in back scattering geometry (stars in Figure 1c).

The hydrodynamic radius of the micelles formed by the ABA triblock copolymer below the LCST is smaller than the one of the PS-*b*-PNIPAM diblock copolymer studied by us previously.[30] This diblock copolymer had block molar masses of 5000 and 18000 g mol^{-1} for PS and PNIPAM, respectively, and at 20 °C, the hydrodynamic radius of the micelles was 40 nm, despite the lower overall molar mass. The geometric effect of the polymer architecture - star-like vs. flower-like micelles - should not have a significant effect on the shell thickness, since the molar mass of the PNIPAM block in the diblock copolymer (18000 g mol^{-1}) is roughly one half of the one of the triblock copolymer (44000 g mol^{-1}). We attribute the discrepancy to a difference in core size and, therefore, in aggregation number. We expect the ABA triblock copolymer micelles to have a smaller core than the diblock copolymer micelles due to the shorter hydrophobic blocks in the triblocks. The decrease of R_h with increasing temperature towards the LCST has been previously observed with di- and ABA triblock copolymers from PS and PNIPAM.[26,28,30] This may be due to the initial stretching of the PNIPAM loops because of the limited area at the surface of the P(S-d_8) core which relaxes partly upon heating.

The clustering above the collapse transition is easily explained by the increased hydrophobicity of the formerly hydrophilic PNIPAM block. It is noteworthy that - at least on the time scale of the investigation - the aggregation stops at a given, relatively well-defined size and leads to stable colloidal aggregates, but does not result in flocculation as observed for the homopolymer.[8] Clusters of similar size ($R_h = 70$–90 nm) have been observed with the above-mentioned PS-*b*-PNIPAM diblock copolymer as well.[30] However, in the diblock copolymer, they were only observed above 40 °C, whereas, in the ABA triblock copolymer, they form right above the collapse transition, and singly-collapsed micelles cannot be detected. We conclude that the ability of the ABA triblock copolymer to bridge two micellar cores[34–36] results in more pronounced cluster formation than in the diblock copolymer where the clusters are only connected by hydrophobic interactions. Only in very dilute solutions ($<10^{-3}$ mg mL^{-1}) of PS-*b*-PNIPAM-*b*-PS triblock copolymers, having significantly lower PNIPAM weight fractions, the collapse of single micelles could be observed.[28]

Inner Structure and Correlation of the Micelles

In order to characterize the inner structure of the micelles, the collapse of the micellar shell and the correlation of the micelles as a function of temperature, we have carried out SANS measurements. By contrast matching the P(S-d_8) core or the PNIPAM shell with the appropriate D_2O/H_2O mixtures, we gained separate information on the core and the shell. By investigating a solution with a relatively low concentration (50 mg mL^{-1}), we could characterize the micelles in the absence of strong correlation. Solutions with a higher concentration (170 mg mL^{-1}) enabled us to investigate the correlations between the micelles as well as their changes at the LCST. Representative SANS curves are shown in Figure 2.

Below the LCST, the curve from the 50 mg mL^{-1} solution in D_2O/H_2O (Figure 2a) is expected to show the scattering from

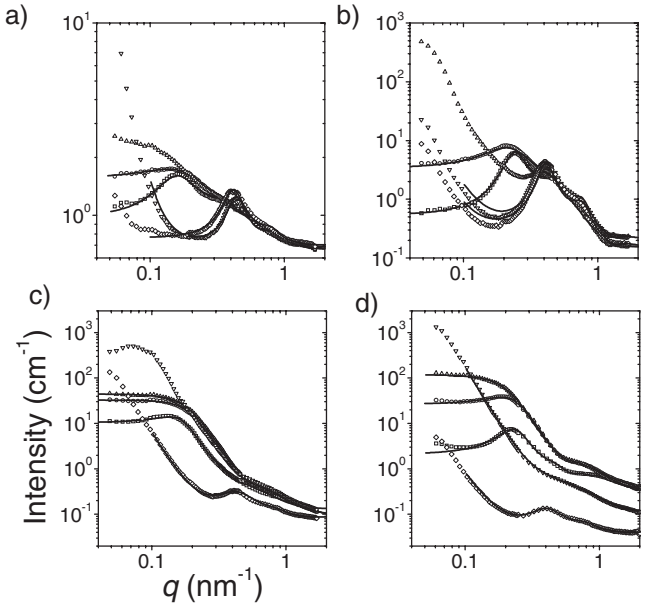

Figure 2.
Representative SANS curves of P(S-d_8)-*b*-PNIPAM-*b*-P(S-d_8): (a) 50 mg mL^{-1} in D_2O/H_2O, (b) 170 mg mL^{-1} in D_2O/H_2O, (c) 50 mg mL^{-1} in D_2O and (d) 170 mg mL^{-1} in D_2O. Experimental curves: (square) 20 °C, (circle) 31 °C, (triangle up) 32 °C, (triangle down) 33 °C, (diamond) 40 °C. The lines are fits, see text. The curves at 35 °C and 40 °C have in some cases lower overall intensities which we attribute to incipient macroscopic phase separation.

weakly interacting micellar P(S-d_8) cores, since the PNIPAM shell is contrast-matched by the solvent. Between 20 and 31 °C, we observe the micellar form factor together with a weak structural peak at 0.16 nm^{-1}, indicating a certain correlation already at this concentration, which may be due to bridging of micelles by the two P(S-d_8) end-blocks. Such a correlation was not observed with the PS-*b*-PNIPAM diblock copolymers studied previously.[30] Fitting of a homogeneous sphere representing the P(S-d_8) core was not successful, and it was necessary to include scattering from the shell which was accomplished by using a core-shell model. In the entire temperature range, the core radius amounts to $R_{core} = 3.3 \pm 0.4$ nm (Figure 3a). Between 20 and 31 °C, the micellar radius R_{mic} increases from 6.7 nm to 13.3 nm, and then abruptly decreases to 3.3 ± 0.2 nm (Figure 3b). The value of R_{mic} below the LCST presumably does not reflect the entire micellar shell but only the inner, dense part, which is visible despite the contrast matching, possibly due to slightly biased contrast matching or to H/D exchange between the amide group in PNIPAM and D_2O. Above the LCST, the partially deuterated, collapsed PNIPAM shell cannot be distinguished from the P(S-d_8) core any more. The hard-sphere radius, which corresponds to half the distance between micelles, is $R_{HS} = 16.3 \pm 1.0$ nm below the LCST (Figure 3c). The large difference between R_{mic} and R_{HS} is another indication that only the inner part of the PNIPAM shell contributes to the scattering and that the micelles presumably have a radius close to R_{HS}.

Heating the solution above 31 °C leads to a drastic increase of forward scattering together with a shift of the correlation peak to a significantly higher q-value, 0.44 nm^{-1}, i.e. the distance between the micelles decreases and clusters are formed due to the collapse of the shell. The forward scattering follows approximately a Porod law, $I(q) \propto q^{-4}$, i.e. the clusters are compact objects. R_{core} has the same value as below the LCST, whereas the apparent R_{mic} decreases abruptly to ~3.3 nm, reflecting the expected collapse of the shell. R_{HS} decreases abruptly to 7.4 ± 0.2 nm. Thus, the distance between the micelles decreases by 55% when heating through the LCST.

The scattering from a solution of the same concentration in D_2O (Figure 2c) is dominated by the responsive PNIPAM shell. Below the LCST, the structure factor is located at the same q-value as in D_2O/H_2O, but it is less visible because of the high value of the form factor of the shell-dominated scattering in this q-region. From the analysis, $R_{core} = 2.6 \pm 0.5$ nm is obtained over the entire temperature range. R_{mic} is 17.2 ± 0.5 nm below and 4.8 ± 0.6 nm above the LCST, i.e. the shell thickness decreases by 85%. R_{HS} decreases from 16.3 ± 0.8 nm below to 6.1 ± 0.9 nm above the LCST, i.e. by 63%. These values are very similar to

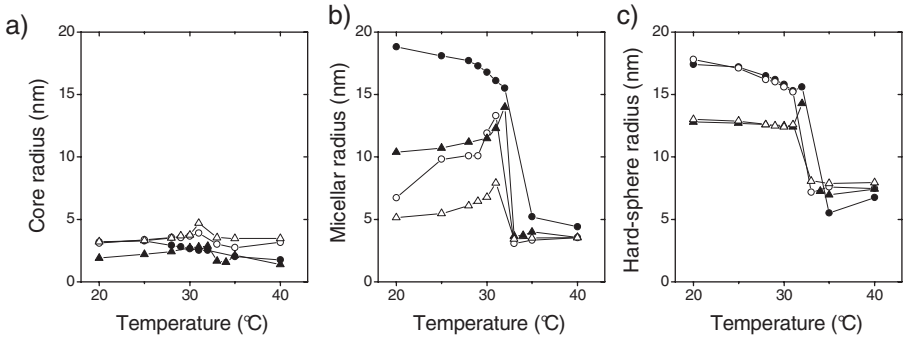

Figure 3.
Results from the fits to the SANS curves in Figure 2: (a) core radius, (b) micellar radius, (c) hard-sphere radius. (Open circles) 50 mg mL^{-1} in D_2O/H_2O, (filled circles) 50 mg mL^{-1} in D_2O, (open triangles) 170 mg mL^{-1} in D_2O/H_2O, (filled triangles) 170 mg mL^{-1} in D_2O. The lines are guides to the eye.

Table 1.
Molar mass characteristics of the synthesized polymers.

Entry	Polymer made	RAFT agent	Yield (%)	M_n^{theor} [a]	M_n (SEC)[b]	PDI [b]	M_n (UV)[c]
1[d]	macroCTA1	CTA1	40	2290	2300	1.19	–
2[e]	P(S-d_8)-*b*-PNIPAM-*b*-P(S-d_8)	macroCTA1	80	35000	19700[f]	1.47	46300

[a] Calculated assuming 100% blocking efficiency and that the molar mass of the P(S-d_8) block corresponds to the one of the macroRAFT agent used. [b] In dimethylacetamide based on polystyrene standards. [c] From the absorbance at 262 nm, assuming that the molar mass of the P(S-d_8) block corresponds to the one of the macroRAFT agent used. [d] Polymerization conditions: 0.089 mol styrene, 2.0×10^{-3} mol RAFT agent, 110 °C, 19 h. [e] Polymerization conditions: 0.044 mol NIPAM, 1.25×10^{-4} mol RAFT agent, 1.5625×10^{-5} mol AIBN, 65.0 °C, 62 h. [f] Apparent value only.

those obtained in D_2O/H_2O. R_{mic} is similar to R_{HS} over the entire temperature range, as expected for micelles which are connected by ABA triblock copolymers bridging two P(S-d_8) cores.

Solutions of higher concentration (170 mg mL^{-1}) show the same overall behavior (Figure 2b,d). The scattering intensities are higher, due to the increased concentration. The correlation peaks are more pronounced than at lower concentration, i.e. a higher fraction of micelles are correlated. A striking difference is that, in D_2O solution, R_{mic} below the LCST (11.7 ± 1.3 nm) is significantly lower than at lower concentration (17.2 ± 1.1 nm) which may be attributed to the higher degree of bridging of the micelles at the higher concentration, hampering the full swelling. Moreover, the temperature behavior is reversed (Figure 3b): At low concentration, R_{mic} decreases with heating to the LCST, in consistency with R_h (Figure 1b), whereas for high concentration, it stays rather constant up to 30 °C and increases abruptly between 31 and 32 °C. This may be a collective effect close to the phase transition. R_{HS}, on the other hand, stays constant over the entire temperature range below the LCST for both contrasts (12.9 ± 0.7 nm in D_2O and 12.7 ± 0.2 nm in D_2O/H_2O). Again, the value is smaller than for low concentration.

Above the LCST, all radii are very similar to those at low concentration. In D_2O solution, R_{mic} decreases to 4.8 ± 0.6 nm (Figure 3b). The shell thickness thus decreases from 9.5 nm to 1.5 nm, a shrinkage of 84%, which is similar to the value obtained with the lower concentration. R_{HS} decreases to 7.2 ± 0.2 nm (in D_2O) or 8.0 ± 0.1 nm (in D_2O/H_2O), also similar to the values at lower concentration. The shrinkage of the micellar distance thus amounts to 44% in D_2O and to 37% in D_2O/H_2O.

Conclusion

We conclude that P(S-d_8)-*b*-PNIPAM-*b*-P(S-d_8) triblock copolymers in aqueous solution form spherical flower-like micelles of core-shell type. The collapse transition at 31–32 °C is fully reversible with a hysteresis between 27 and 37 °C, and the clustering of the collapsed micelles is a two-step process, as evidenced by turbidimetry. The hydrodynamic radius of the micelles decreases from 29 nm to 21 nm, when heating from 20 °C to the LCST; above the LCST, only clusters from collapsed micelles are observed in DLS. The core radius is ~2.9 nm, independent of temperature as expected for P(S-d_8) in water. The aggregation number calculated from the ratio of the average core volume and the volume of two P(S-d_8) blocks, is $N_{agg} = 32 \pm 18$, which is in the expected range. These values lead to an area of only 1.65 nm^2 per PNIPAM strand, i.e. they are in a brush conformation.[37] The PNIPAM shell thickness as well as the hard-sphere radius decrease with increasing concentration, which we attribute to the increased amount of bridging between micelles in the more concentrated solution. The shell collapses at the LCST and has a very small thickness above the LCST (~2 nm). The strong forward scattering above the LCST is due to the formation of large clusters consisting of collapsed

core-shell micelles. At this, the hard-sphere radius, i.e. the distance between the micelles, decreases abruptly at the LCST with the amount depending on concentration: it shrinks by ~60% at 50 mg mL^{-1}, but only by ~41% at 170 mg mL^{-1}, the reason being the lower value of the micellar distance below the LCST for the higher concentration. The clusters are compact as evidenced by the decay of the forward scattering which follows a Porod law reasonably well. The core-shell structure of the micelles is preserved even within the clusters with very low shell thicknesses (~2 nm).

We note that the overall behavior of the ABA triblock copolymer is similar to the one of the PS-*b*-PNIPAM diblock copolymer studied by us previously.[30] However, the micellar cores of the diblock copolymer are much larger ($R_{core} = 11.1$ nm at 20 °C), and the aggregation number is significantly higher ($N_{agg} = 724$). We attribute this to the longer PS blocks (5000 g mol^{-1}) and the star-like micellar conformation, in contrast to the flower-like conformation of the micelles formed by the ABA triblock copolymers. The collapse transition of the diblocks shows a two-step process in turbidimetry as well. However, with the diblock copolymers, clusters are only detectable far above the LCST, and a correlation between micelles is only observed above the LCST. These observations indicate the importance of bridging which is possible only in the ABA triblock copolymers.

Acknowledgements: We thank W. Doster, V. Pipich and A. Golosova for assistance with the experiments and fruitful discussions. We kindly acknowledge given beam time by the Jülich Centre for Neutron Science at FRM II. This work was supported by the DFG priority program ''Intelligente Hydrogele'' (Pa771/4, Mu1487/8, La611/7). A.M.B.K. gratefully acknowledges a personal grant from Deutscher Akademischer Austauschdienst (DAAD).

[1] M. Das, H. Zhong, E. Kumacheva, *Ann. Rev. Mater. Res.* **2002**, *36*, 117–311.
[2] A. S. Hoffman, *J. Controlled Release* **1987**, *6*, 297–305.
[3] D. C. Coughlan, F. P. Quilty, O. I. Corrigan, *J. Controlled Release* **2004**, *98*, 97–114.
[4] D. Schmaljohann, *Adv. Drug Deliv. Rev.* **2006**, *58*, 1655–1670.
[5] H. Feil, Y. H. Bae, J. Feijen, S. W. Kim, *J. Membrane Sci.* **1991**, *64*, 283–294.
[6] Y. S. Park, Y. Ito, Y. Imanishi, *Langmuir* **1998**, *14*, 910–914.
[7] A. Nykänen, M. Nuopponen, A. Laukkanen, S.-P. Hirvonen, M. Rytelä, O. Turunen, H. Tenhu, R. Mezzenga, O. Ikkala, J. Ruokolainen, *Macromolecules* **2007**, *40*, 5827–5834.
[8] H. G. Schild, *Prog. Polym. Sci.* **1992**, *17*, 163–249.
[9] S.-Y. Lin, K.-S. Chen, L. Run-Chu, *Polymer* **1999**, *40*, 2619–2624.
[10] Y. Katsumoto, T. Tanaka, H. Sato, Y. Ozaki, *J. Phys. Chem. A* **2002**, *106*, 3429–3435.
[11] Y. Hirokawa, T. Tanaka, E. S. Matsuo, *J. Chem. Phys.* **1984**, *81*, 6379–6380.
[12] M. Shibayama, T. Tanaka, C. C. Han, *J. Chem. Phys.* **1992**, *97*, 6829–6841.
[13] G. Liao, Y. Xie, K. F. Ludwig, Jr., R. Bansil, P. Gallagher, *Phys. Rev. E* **1999**, *60*, 4473–4481.
[14] R. H. Pelton, P. Chibante, *Colloids Surf.* **1986**, *20*, 247–256.
[15] T. Hellweg, K. Kratz, S. Pouget, W. Eimer, *Coll. Surf. A* **2002**, *202*, 223–232.
[16] M. Stieger, J. S. Pedersen, P. Lindner, W. Richtering, *Langmuir* **2004**, *20*, 7283–7292.
[17] S. Höfl, L. Zitzler, T. Hellweg, S. Herminghaus, F. Mugele, *Polymer* **2007**, *48*, 245–254.
[18] N. Dingenouts, C. Norhausen, M. Ballauff, *Macromolecules* **1998**, *31*, 8912–8917.
[19] T. Hellweg, C. D. Dewhurst, W. Eimer, K. Kratz, *Langmuir* **2004**, *20*, 4330–4335.
[20] M. Anderson, S. Hietala, H. Tenhu, S. L. Maunu, *Colloid Polym. Sci.* **2006**, *284*, 1255–1263.
[21] I. Berndt, J. S. Pedersen, W. Richtering, *Angew. Chem. Int. Ed.* **2006**, *45*, 1737–1741.
[22] P. Kujawa, H. Watanabe, F. Tanaka, F. M. Winnik, *Eur. Phys. J. E* **2005**, *17*, 129–137.
[23] W. Wang, K. Troll, G. Kaune, E. Metwalli, M. Ruderer, K. Skrabania, A. Laschewsky, S. V. Roth, C. M. Papadakis, P. Müller-Buschbaum, *Macromolecules* **2008**, *41*, 3209–3218.
[24] M. Nuopponen, J. Ojala, H. Tenhu, *Polymer* **2004**, *45*, 3643–3650.
[25] M. Mertoglu, S. Garnier, A. Laschewsky, K. Skrabania, J. Storsberg, *Polymer* **2005**, *46*, 7726–7740.
[26] W. Zhang, X. Zhou, H. Li, Y. Fang, G. Zhang, *Macromolecules* **2005**, *38*, 909–914.
[27] T. Tang, V. Castelletto, P. Parras, I. W. Hamley, S. M. King, D. Roy, S. Perrier, R. Hoogenboom, U. S. Schubert, *Macromol. Chem. Phys.* **2006**, *207*, 1718–1726.
[28] X. Zhou, X. Ye, G. Zhang, *J. Phys. Chem. B* **2007**, *111*, 5111–5115.
[29] S. E. Kirkland, R. M. Hensarling, S. D. McConaughty, Y. Guo, W. L. Jarrett, C. L. McCormick, *Biomacromolecules* **2008**, *9*, 481–486.

[30] K. Troll, A. Kulkarni, W. Wang, C. Darko, A. M. Bivigou Koumba, A. Laschewsky, P. Müller-Buschbaum, C. M. Papadakis, *Colloid Polym. Sci.* **2008**, *286*, 1079–1092.
[31] J. Jakeš, *Coll. Czech. Chem. Commun.* **1995**, *60*, 1781–1791.
[32] S. Förster, C. Burger, *Macromolecules* **1998**, *31*, 879–891.
[33] Y. Ding, X. Ye, G. Zhang, *Macromolecules*. **2005**, *38*, 904–908.
[34] A. N. Semenov, J.-F. Joanny, A. R. Khokhlov, *Macromolecules* **1995**, *28*, 1066–1075.
[35] P. Kujawa, F. Segui, S. Shaban, C. Diab, Y. Okada, F. Tanaka, F. M. Winnik, *Macromolecules* **2006**, *39*, 341–348.
[36] R. Nojima, T. Sato, X. Qiu, F. M. Winnik, *Macromolecules* **2008**, *41*, 292–294.
[37] H. Yim, M. S. Kent, S. Mendez, G. P. Lopez, S. Satija, Y. Seo, *Macromolecules* **2006**, *39*, 3420–3426.

